JOURNAL OF NATURAL REMEDIES
DOI: 10.18311/jnr/2025/49463
RESEARCH ARTICLE

Green Synthesis of Silver Nanoparticles Using *Terminalia arjuna* Extract and their Antibacterial Activity Against ESBL-producing *Escherichia coli*

P. Senthilkumar* and J. Rengaramanujam

Department of Microbiology, Dr. N.G.P Arts and Science College, Bharathiyar University, Coimbatore - 641048, Tamil Nadu, India; microsenthilphd@gmail.com

Abstract

Background: The emergence of resistance among *Escherichia coli* bacteria, particularly those expressing extended-spectrum beta-lactamase enzymes, poses a significant threat to successful antibiotic treatment. Natural plant-based compounds with nanotechnology offer a sustainable method for generating alternative antibacterial agents. **Aim:** The objective of this study was to generate silver-based nanoparticles using the aqueous extract of *Terminalia arjuna* and assess their antibacterial efficacy against drug-resistant *E. coli*. **Methods**: Bacterial isolates were identified using conventional microbiological methods such as Gram staining, growth characteristics on MacConkey agar, and biochemical testing. Antimicrobial susceptibility was determined using the disc diffusion method in compliance with clinical laboratory guidelines. Resistance genes were detected using a polymerase chain reaction. Silver-based nanoparticles were created using green synthesis by combining an aqueous extract of *T. arjuna* with silver nitrate solution. Analytical techniques such as ultraviolet-visible spectroscopy, infrared spectroscopy, crystal structure analysis, scanning and transmission electron microscopy, and elemental composition analysis was used for confirmation of nanoparticle. The antibacterial activity was assessed using the agar well diffusion assay. **Results:** Four of the six bacterial isolates had high resistance to beta-lactam antibiotics and were found to have resistance-related genes. The synthesised nanoparticles were spherical in shape, with an average size of 30 to 35 nanometres and mean zeta potential value of -33.6 mV. Elemental analysis verified the presence of silver as its primary component. The silver-based nanoparticles exhibited potent antibacterial action, with inhibition zones rising proportionately with concentration and reaching up to 18.50±0.50 mm at the highest dose and MIC of 125µg/ml. The silver nanoparticles exhibited moderate cytotoxicity with an IC_{50} value of 74.236 µg/mL in Vero cell lines. Concentrations below this threshold were found to be biocompatible, indicating potential for safe antibacterial applications. **Conclusion:** This study demonstrates the successful green synthesis and characterisation of silver nanoparticles using *T. arjuna* extract. Their proven antibacterial effectiveness against resistant *E. coli*, along with their biocompatibility, encourages more research into potential therapeutic and pharmacological uses.

Major Findings: The green synthesis of silver-based nanoparticles with *T. arjuna* extract provides an effective friendly alternative for treating multidrug-resistant *E. coli*, indicating their potential use in future antimicrobial therapeutics.

Keywords: Antibiotic Resistance, *E. coli,* ESBL, MDR, Silver Nanoparticles*, T. arjuna*

1. Introduction

The emergence of antibiotic resistance in infectious disease-causing microbes has presented greater challenges to both the economy and public health. To treat bacterial illnesses, 100,000 tons of antibiotics are manufactured each year. A new antibiotic that is effective against Multidrug-Resistant (MDR) bacteria is desperately needed, as current medicines have not been able to control MDR germs. MDR is defined as resistance with a value of ≥1 antimicrobial agent in 3 or more antimicrobial categories. A number of processes, including chemical changes and antibiotic agent

*Author for correspondence

Article Received on: 16.04.2025 Revised on: 11.07.2025 Accepted on: 20.08.2025

degradation, decreased antibiotic penetration through protein modification and efflux pump application, target site modification through enzymatic and mutational changes, and resistance gene acquisition, can lead to the development of MDR[1].

Nanotechnology has recently offered a fresh approach to combating multidrug-resistant bacteria. Because of their distinct qualities over their bulk counterparts, Metal Nanoparticles (MNPs) smaller than 100 nm in various forms were successfully used. Depending on the physicochemical characteristics of each metal element, MNPs such Ag, Cu, Fe_3O_4, TiO_2, and ZnO have demonstrated varying antibacterial activity. MNPs and AgNPs outperformed the others in terms of antibacterial activity through a variety of methods. MNPs size and form, in addition to their basic structure, are crucial in this activity[2]. Since metal and metal oxide nanoparticles have such good qualities as a high surface to volume ratio and great dispersion in solution, among other advantages, they have been the subject of much scientific and technological investigation among all other forms of NPs. Because of this, metal and metal oxide nanoparticles have improved antibacterial capabilities[3].

Green synthesis methods are progressively replacing physical and chemical processes due to concerns about high energy consumption, release of hazardous compounds, need for advanced machinery, and synthesis conditions[4]. Green synthesized metal nanoparticles may exceed chemically synthesized ones in certain conditions. When opposed to chemical and physical processes, green synthesis offers several benefits, including being non-toxic, pollution-free, ecologically friendly, cost-effective, and more sustainable. Proteins and polyphenols that exist in green materials can act as reducing agents in place of chemical reagents, decreasing the valence state of metal ions. Metal nanoparticles may be produced with green materials and under the right parameters (temperature, concentration, air quality, *etc.*)[5].

Terminalia arjuna is a member of the family *Combretaceae*. It is a 20-30 m tall tree that grows in Sri Lanka, India, and Burma. Heart failure, hypercholesterolemia, and coronary artery disease have all been treated using *T. arjuna* bark stem powder. Arjunic acid, arjugenin, arjunetin, arjunoglucoside, flavonoids, triterpenoids, and tannins were isolated from *T. arjuna* bark, according to phytochemical analyses. Leucoanthocyanidins and hydrolysable tannins are present in the leaf extract, whereas saponins, flavonoids, glycosides, and polyphenolic compounds are present in the fruit extract[6].

This study describes the environmentally friendly synthesis and characterization of Ag NPs utilizing *T. arjuna* leaf extract. Using clinical isolates of *E. coli* MDR strains, the antibacterial effectiveness of the characterized nanoparticles was assessed.

2. Materials and Methods

2.1 Sample Collection

The clinical isolates were procured from primary healthcare, Coimbatore and then taken to the lab for bacteriological examination in a thermobox at 4°C.

2.2 Bacterial Identification

Loopfuls of enriched buffered peptone water (HiMedia) from positive tubes (turbid appearance of bacterial growth from nasal swabs) were then streaked over MacConkey agar (HiMedia M317) and cultured for 18 to 24 hours at 37°C in order to isolate *E. coli*. Other physiological and biochemical tests, including Gram staining, IMVIC (Indole, Methyl red, Voges-Proskauer), oxidase, and H_2S were subsequently used to further characterize the identified *E. coli*.

2.3 Determination of Antibiotic Susceptibility

In accordance with CLSI recommendations, the disc diffusion technique was utilized to determine the *E. coli* isolates sensitivity to various antibiotics. Cefotaxime-30µg, Ceftriaxone-10µg, Gentamicin-10µg, Ciprofloxacin-5µg, Norfloxacin-10µg, Colistin-10µg, Amoxicillin + clavulanic acid-30µg, Cotrimoxazole-25µg, Amoxycillin-10µg, Amikacin-30µg, Furazolidon-50µg, Netilmicin-30µg were the discs used[7].

2.4 Molecular Detection of ESBLs

In the traditional DNA extraction approach, colonies were picked and dissolved in 500µl lysis buffer, which contained 50µg of proteinase K, as well as in EDTA (0.05 M), SDS (I%), Nacl (1.168%), and Tris (0.02 M). The solution was vortexed with an equivalent amount

Table 1. Primer sequences of target genes

	Primer Sequence	Fragment Size (bp)
bla_{TEM}(F)	TTGGGTGCACGAGTGGGTTA	873
bla_{TEM}(R)	TAATTGTTGCCGGGAAGCTA	
bla_{CTX-M} (F)	ATGTGCAGYACCAGTAARGTKATG GC	592
bla_{CTX-M} (R)	TGGGTRAARTARGTSACCAGAAYCAGC GG	

of phenol chloroform isoamyl alcohol (50:49:1) after being incubated for two hours at 65° C. It was then centrifuged for 15 minutes at 5000 rpm. An equivalent amount of chloroform was used to wash the supernatant, and 0.7 volumes of isopropanol were used to precipitate the DNA. The lμL used for PCR was added to 24μL of PCR solution after the dried pellet had been redissolved in 15μL of TE buffer[8].

The amplification of resistance genes was performed with specific primers for *bla*TEM, *bla*CTX-M15 μL of Master Mix (SRL chemicals), 0.3 μM of each primer, and 0.1 to 0.5 ng/μL of isolated DNA were used for the amplification process. PCR was performed in a thermal cycler with the following cycling conditions for blaCTX-M: Initial denaturation at 94° C for 7 min, followed by 35 cycles of amplification with denaturation at 94° C for 30 s, annealing at 57° C for 30 s, and extension at 72° C for 30 s, followed by a final extension at 72° C for 5 minutes. The blaTEM gene's annealing temperature was 53°C[9]. PCR was carried out using the primer sequence listed in Table 1.

2.5 Collection and Extraction of Plant Extract

The leaves of *T. arjuna* (*Combretaceae*) were collected from Cauvery river-forests. The leaves were collected, washed thoroughly with tap water and distilled water. They were shade-dried, uniformly powdered and subjected to sequentially extraction by water. The extracts were concentrated under reduced pressure, using rotary evaporator. The dried crude concentrated extracts were weighed to calculate the extractive yield and stored in a refrigerator in air-tight bottles, until used for analysis[10].

2.6 Green Synthesis of Nanoparticles

Silver nanoparticles (AgNPs) were synthesized using aqueous leaf extract of *T. arjuna* as reducing and stabilizing agents. For each synthesis, 80 mL of 50 mM $AgNO_3$ solution was mixed with 20 mL of 20% (w/v) freshly prepared plant extract under continuous stirring at 450 rpm and 25 ± 1°C for 3 hours. The pH was maintained at 9.0 ± 0.2 using 0.1 N NaOH/HCl. The formation of AgNPs was indicated by a color change and confirmed by UV-Vis absorption. The reaction mixture was centrifuged at 10,000 rpm for 15 minutes at 4° C, washed thrice with 90% ethanol, and dried at 80° C for 2 hours to obtain powdered AgNPs. The synthesis was carried out in several batches throughout the study for various assays. The batch uniformity was checked using UV-Vis spectra, pellet weight, and visual appearance. Only consistent batches were chosen for further characterization[11].

2.7 Characterization of Nanoparticle

The synthesized nanoparticle using plant extract was evaluated using a UV-Vis spectrophotometer programmed to scan wavelengths between 300 and 800 nm, the absorption peak was found. An instrument used for this study was a Perkin-Elmer Lambda 25 spectrophotometer[12]. For the morphological analysis, a scanning electron microscope (FEI Nova Nano SEM 450, USA) was utilized. The SEM verified the size, shape, and crystalline nature of the silver nanoparticles[13]. An FTIR/ATR spectrophotometer from Perkin Elmer was used to characterize the nanoparticles that were biosynthesized. The 400 cm-1 to 4000 cm-1 spectral range was covered by this investigation. The biomolecules in charge of the reduction of metal ions and the encapsulating of the resultant nanoparticles were identified using Fourier Transform Infrared (FTIR) spectroscopy[14]. The nanoparticles decreased by plant extract were analyzed using X-ray Diffraction (XRD) by evenly placing the dried NPs onto an XRD grid. After that, the spectrum was captured using a Philips PW 1830 X-Ray generator that was employing Cu Kα1 radiation and running at a voltage of 40 kV and

a current of 30 mA[15]. The NPs samples were analyzed using Energy Dispersive X-ray spectroscopy (EDX) for qualitative elemental studies. The zeta potential of the synthesized silver nanoparticles was determined using a Malvern Zetasizer (Model: MAL1111244). In a clear disposable zeta cell, measurements were taken at 25°C using ethanol as the dispersant[16].

2.8 Antibacterial Activity of Nanoparticle

2.8.1 Zone of Inhibition Assay

Using the agar well diffusion method, isolated compounds were examined for antibacterial activity in Mueller Hinton Agar (MHA) plates. *E. coli* ESBL the test organisms, were injected in nutritional broth and grown overnight at 37°C to produce a final inoculum of $1.5 \cdot 10^8$ CFU/ml. This allowed the turbidity to be adjusted to 0.5 McFarland. Standardized microbial culture broth was used to produce MHA plates. Using the appropriate solvents, compounds with concentrations of 1000, 500, 250, and 100 µg/ml were created[17].

2.8.2 Minimum Inhibitory (MIC) and Bactericidal Concentration (MBC)

The antibacterial activity of silver nanoparticle was evaluated using the broth dilution method, following CLSI guidelines. Test bacteria (*E. coli* ESBL) were inoculated into Mueller-Hinton broth and incubated at 37°C for 18-24 hours. Nanoparticle was prepared in DMSO at 1000 µg/mL and serially 2-fold diluted in a 96-well plate containing MHB. A standardised bacterial suspension (0.5 McFarland) was added to each well and incubated. MIC was recorded as the lowest concentration showing no visible growth. For MBC, samples from non-turbid wells were spread on Mueller-Hinton agar and incubated at 37°C for 24 hrs[18].

2.9 Cell Cytotoxicity

The cytotoxic effect of nanoparticle on Vero cells (NCCS) was evaluated using the MTT assay. Vero cells were maintained in Dulbecco's Modified Eagle Medium (DMEM) containing 10% fetal bovine serum with penicillin, and streptomycin. Cells were incubated at 37° C in a humidified 5% CO_2 atmosphere. After reaching appropriate confluency, they were trypsinized, centrifuged, and resuspended in fresh medium. A cell suspension of 10^5 cells/mL was seeded into 96-well plates and incubated for 24 hours. Then nanoparticle was added at varied concentration ranging from 1-512µg/ml MTT solution was added to each well and incubated for 4 hours to allow for formazan crystal formation, which was then solubilised using DMSO. Absorbance was measured at 517 nm, and cell viability percentages were calculated to determine the IC_{50} value compared to untreated controls[19].

2.10 Statistical Analysis

All experiments were performed in triplicates. The analysed data were presented as mean ± SD and ANOVA analysis was performed using GraphPad Prism software (version-8).

3. Results

3.1 Identification of *E. coli* by Conventional Methods

The Extended-Spectrum **β-lactamase (ESBL)**-producing *E. coli* isolates obtained were identified using MacConkey agar, Gram staining, and biochemical tests. On MacConkey agar, ESBL-producing *E. coli* formed medium-sized, smooth, round, lactose-fermenting colonies that appeared pink to red, often with a bile salt precipitate surrounding the colonies, indicating strong lactose fermentation. Gram staining confirmed that the isolates were Gram-negative, appearing as pink, short rod-shaped *bacilli* under the microscope.

Biochemical characterization further confirmed the identity of *E. coli*. The isolates were oxidase-negative, differentiating them from oxidase-positive bacteria like *Pseudomonas*. They were also Voges-Proskauer (VP)-negative and citrate-negative, ruling out *Enterobacter* and *Klebsiella* species. The isolates were Methyl Red (MR)-positive, indicating stable acid production from glucose fermentation. Additionally, they tested positive for catalase and indole production, which are characteristic features of *E. coli*. Notably, hydrogen sulfide (H_2S) production was negative, further distinguishing them from *Salmonella* spp. The pictorial representation of bacterial identification is given in Figure 1.

3.2 Antibiotic Susceptibility Testing

The antibiotic susceptibility testing of six *E. coli* isolates from nasal swabs was analyzed based on Clinical and Laboratory Standards Institute (CLSI) guidelines (Figure 2). Among these 1, 4, 5, and 6 were identified

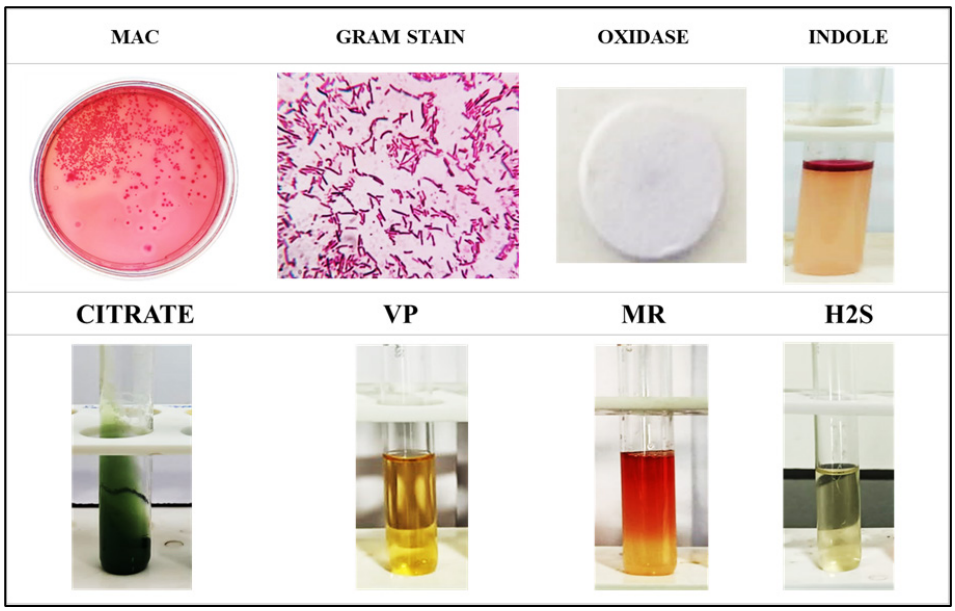


Figure 1. Bacterial identification of ESBL-producing *E. coli* showing characteristic colony morphology and biochemical confirmation.

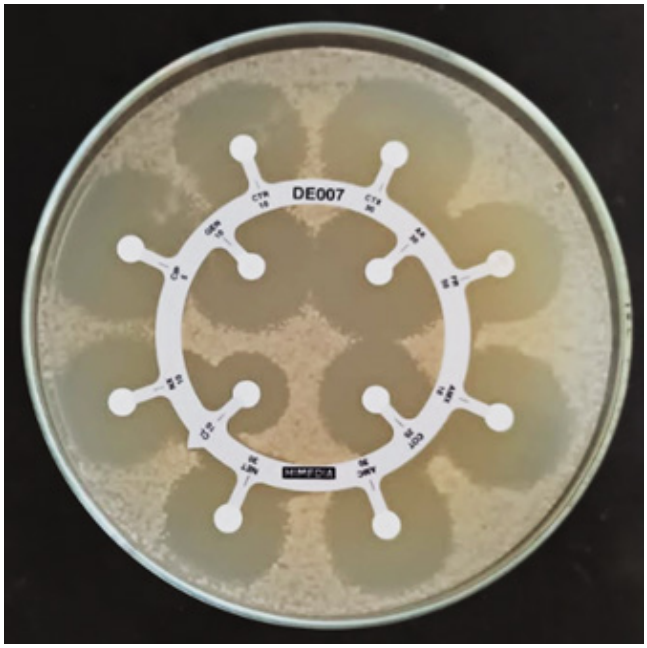


Figure 2. Antimicrobial susceptibility-Dodeca universal combination of 12 antibiotics.

as strong ESBL producers, exhibiting resistance to cefotaxime (≤14 mm) and ceftriaxone (≤14 mm), confirming high β-lactamase activity (Table 2). These isolates also showed intermediate susceptibility to ciprofloxacin (11-12 mm) and norfloxacin (14-15 mm), indicating a moderate level of fluoroquinolone resistance. However, they remained susceptible to colistin (≥17 mm), aminoglycosides such as amikacin (≥16 mm), and netilmicin (≥17 mm). Conversely, 2 and 3 were classified as mild ESBL producers based on their intermediate resistance to cefotaxime (15-16 mm) and ceftriaxone (14-15 mm). These isolates exhibited higher susceptibility to fluoroquinolones, with ciprofloxacin (16-18 mm) and norfloxacin (16-18 mm) showing greater efficacy compared to the strong ESBL producers. Amoxicillin alone showed reduced susceptibility (≤14 mm) in all ESBL- producing isolates, while amoxicillin + clavulanic acid remained effective across all strains (≥20 mm), suggesting the potential efficacy of β-lactamase inhibitor combinations in treatment. Figure 3 represents the bar graph of antibiotics against ESBL strains.

3.3 Identification of ESBL Genes-PCR Analysis

PCR analysis of six ESBL-producing *E. coli* isolates from nasal swabs revealed that 4 strains were positive for both TEM and CTX genes, while 2 were negative (2 and 3). The co-occurrence of these genes indicates a high prevalence of β-lactam resistance, particularly against penicillin and third-generation cephalosporins. TEM-type β-lactamases hydrolyze a broad range of β-lactam antibiotics, while CTX-M-type enzymes exhibit strong activity against cefotaxime and related cephalosporins.

Table 2. Antimicrobial susceptibility testing against ESBL- producing *E. coli*

Antibiotics (µg)	ZOI (mm)					
	1	2	3	4	5	6
Cefotaxime (30 µg)	12.50±0.50	14.30±0.75	16.43±0.51	13.67±1.15	14.00±1.00	11.90±1.15
Ceftriaxone (10 µg)	13.07±1.01	14.00±1.00	15.27±1.66	12.90±1.01	13.73±1.17	12.00±1.00
Gentamicin (10 µg)	17.17±1.76	15.83±1.76	17.03±1.55	14.50±1.80	18.93±0.93	18.53±0.75
Ciprofloxacin (5 µg)	12.20±1.71	12.20±1.31	15.80±0.72	12.20±0.72	12.17±1.26	12.87±1.00
Norfloxacin (10 µg)	17.33±1.53	16.03±1.05	18.60±0.79	14.93±1.01	14.80±1.21	17.37±0.57
Colistin (10 µg)	16.47±1.36	18.37±0.47	19.67±1.53	21.27±1.10	22.70±1.13	19.70±1.87
Amoxicillin + Clavulanic Acid (30 µg)	22.00±1.73	21.20±1.93	20.90±1.15	23.10±0.66	24.77±1.50	23.20±1.06
Cotrimoxazole (25 µg)	14.67±1.53	14.83±1.04	16.00±1.00	14.43±1.25	14.17±1.04	14.80±0.70
Amoxicillin (10 µg)	12.00±1.00	13.73±1.10	15.50±0.46	11.40±1.1.51	12.07±0.55	14.53±0.50
Amikacin (30 µg)	18.50±0.50	17.60±1.04	20.10±0.56	15.80±0.72	21.23±0.68	18.90±1.15
Ceftriaxone (50 µg)	17.03±0.95	18.40±0.53	19.50±1.32	16.80±1.71	18.00±1.00	16.13±1.03
Netilmicin (30 µg)	18.57±1.37	16.17±1.26	18.801.06	14.90±1.32	19.00±1.73	17.67±1.15

Note: Data represents mean values of three replicates ± SD with p value <0.0001.

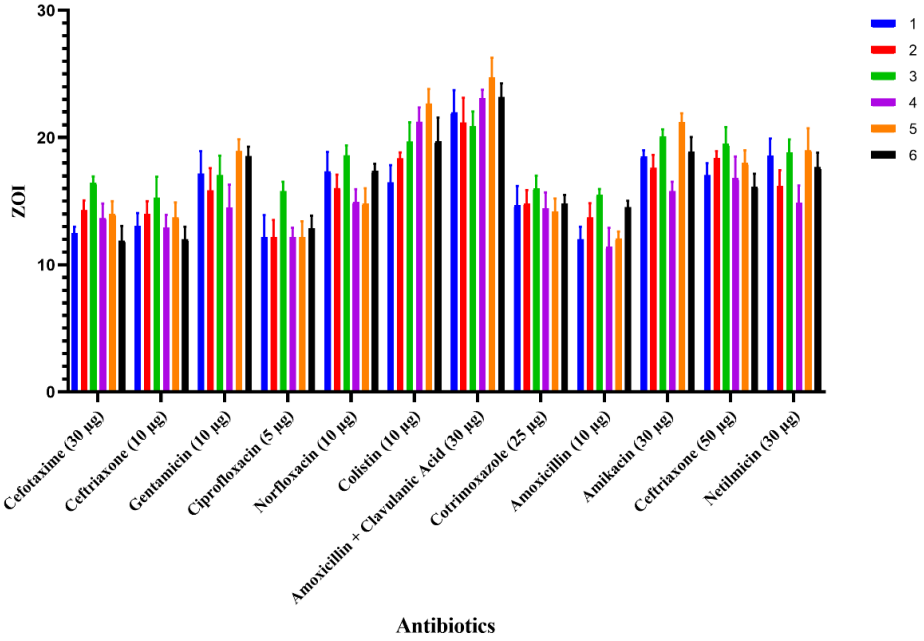


Figure 3. Error bar of zone of inhibition (antibiotics *vs* ESBL strains).

The detection of both genes in the majority of isolates suggests horizontal gene transfer and strong selective pressure for ESBL- mediated resistance. Figures 4 and 5 represent the gel electrophoresis image with ladder (100bp) of CTX-M and TEM, respectively.

3.4 Extraction

Extraction yield of plant material was done using Soxhlet extraction and yield was calculated. Table 3 shows the percentage yield of Soxhlet extraction using aqueous solvent.

3.5 Green Synthesis of Nanoparticle

The silver nanoparticles were green synthesized using *T. arjuna* in the current study. The transformation of the solution colour from clear to dark brown solution served as the first indication that nanoparticle had been successfully synthesized. Wide range of parameters

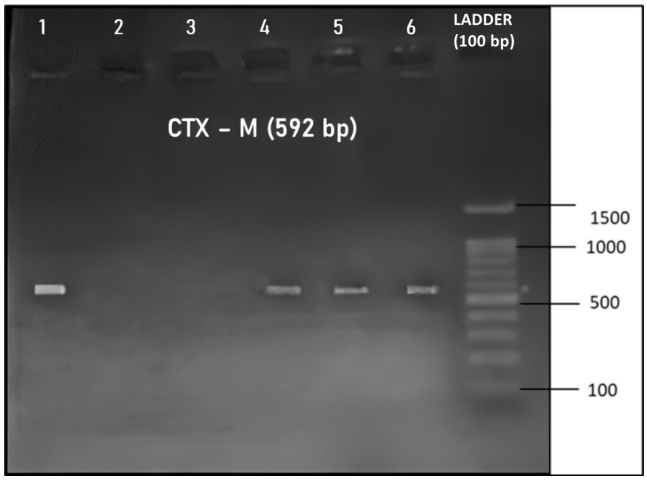


Figure 4. PCR amplification of CTX-M gene- agarose gel electrophoresis.

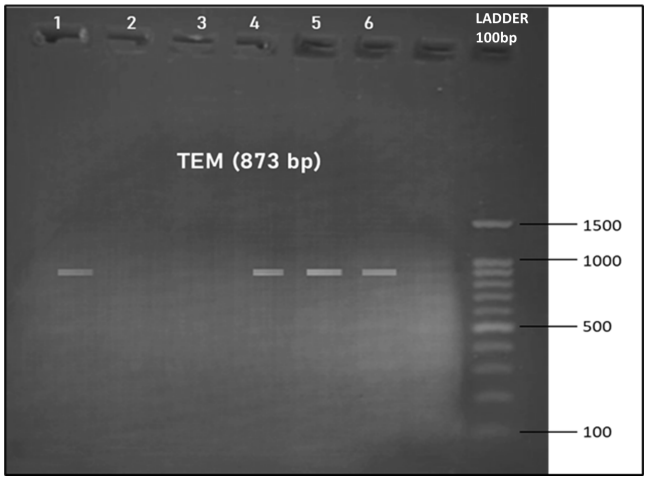


Figure 5. PCR amplification of TEM gene-agarose gel electrophoresis.

Table 3. Extraction yield of *T. arjuna*

S. No.	Plant Name	Solvent Used	Appearance	Extraction Yield (%)
1	*T. arjuna*	Water	Creasy brown	69.43±1.28

Note: Data represents mean values of three replicates ± SD.

can influence nanoparticle formation. The nature of the reductant and the medium in which the reduction is occurring determine how quickly particle formation occurs. The Surface Plasmon Resonance (SPR) in the reaction samples was excited, which resulted in the shift in color. The phyto-compounds (Alkaloids, flavonoids, steroids, phenolic compounds, terpenoids,

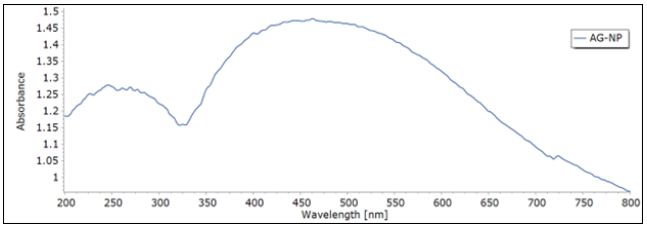


Figure 6. UV-vis absorption spectrum of silver nanoparticles synthesized using *T. arjuna* extract.

and tannins) in the extract of *T. arjuna* served as reducing agents to reduce metal ions into respective nanoparticles.

3.6 Characterization of Nanoparticle

3.6.1 Characterization by Ultra Violet-Visible Spectrophotometer (UV-Vis)

UV-Vis spectrophotometric analysis was conducted to initially investigate the synthesis of silver nanoparticles (AgNPs). A noticeable color change from green to yellowish-brown in the plant extract mixture indicated the formation of *T. arjuna* AgNPs. Spectral analysis revealed a peak for AgNPs at 464 nm and small shoulder at 410 nm (Figure 6), which was the highest observed, and this peak remained stable for several days without further increase in absorption.

3.6.2 Characterization by Fourier Transform Infrared Spectroscopy (FTIR)

FTIR was used to detect the functional groups of *T. arjuna* and silver nanoparticles (Figure 7a and b respectively). The FTIR peaks obtained from *T. arjuna* extract were observed at 3818.36, 3736.4, 3218.61, 2360.44, 2114.56, 1995, 1617.98, 1381.75, 1224.58, 1051.01, and 639.29 cm^{-1}. The FTIR peaks observed for silver nanoparticles synthesized using *T. arjuna* were 3672, 3283, 2915, 2345, 1605, 1501, 1097, 976, and 745 cm^{-1}.

3.6.3 Characterization by X-ray Diffraction (XRD)

The crystallinity of the silver nanoparticles synthesized using *T. arjuna* leaf extract was analyzed *via* XRD (Figure 8). The particle size was determined using the Debye-Scherrer equation: where D is the particle diameter, k is a constant (0.9), is the X-ray wavelength (0.1541 nm), is the Full Width at Half Maximum (FWHM), and is the diffraction angle related to the

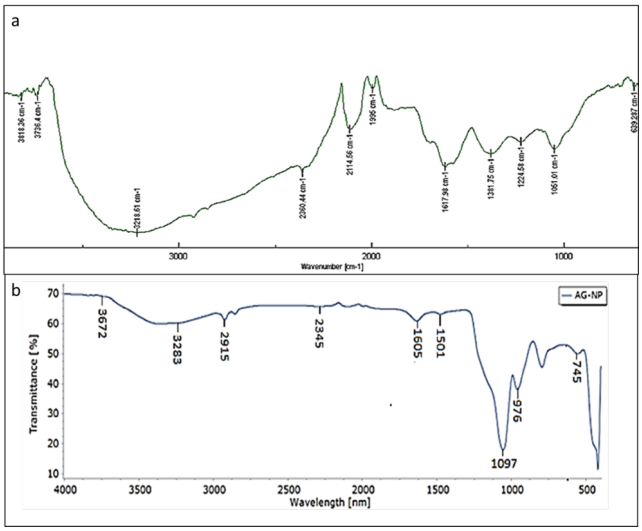


Figure 7. FTIR spectrum of plant extract **(a).** and biosynthesized silver nanoparticles; **(b).** showing major functional groups.

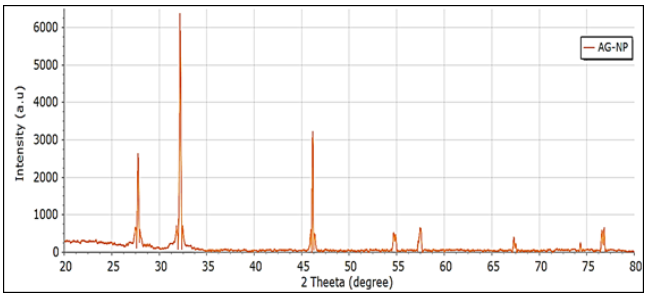


Figure 8. XRD pattern of silver nanoparticles indicating crystalline structure.

(111) lattice planes. The average crystalline size was approximately 30 nm.

3.6.4 Characterization by Transmission Electron Microscopy (TEM)

The TEM analysis (Figure 9) indicates the AgNPs are mostly spherical or quasi-spherical in shape, with dense Ag cores suggesting well-formed crystalline nanoparticles.

3.6.5 Characterization by Scanning Electron Microscopy (SEM)

The size and shape of the produced AgNPs were assessed using a SEM. SEM structural analysis (Figure 10) revealed the presence of flavonoids, amino acids, waxes, antioxidants, and phenolic substances. Particles are primarily spherical in form, with a size

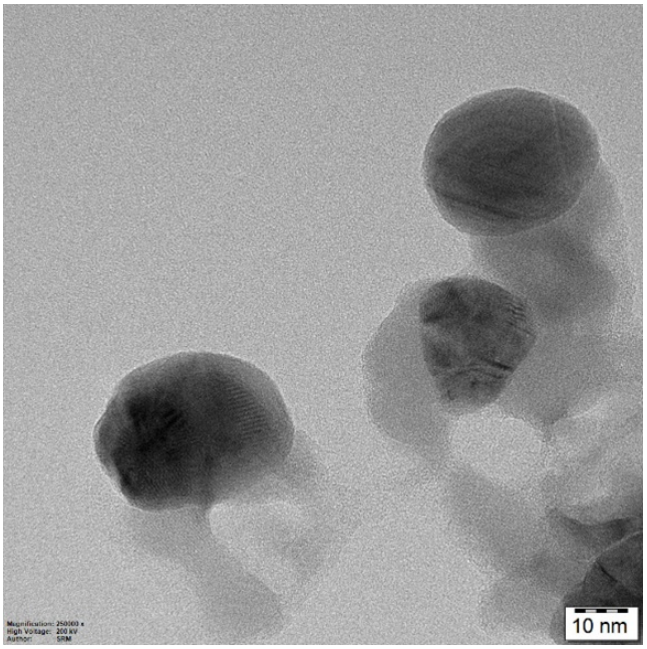


Figure 9. TEM micrograph of silver nanoparticles showing size and shape distribution.

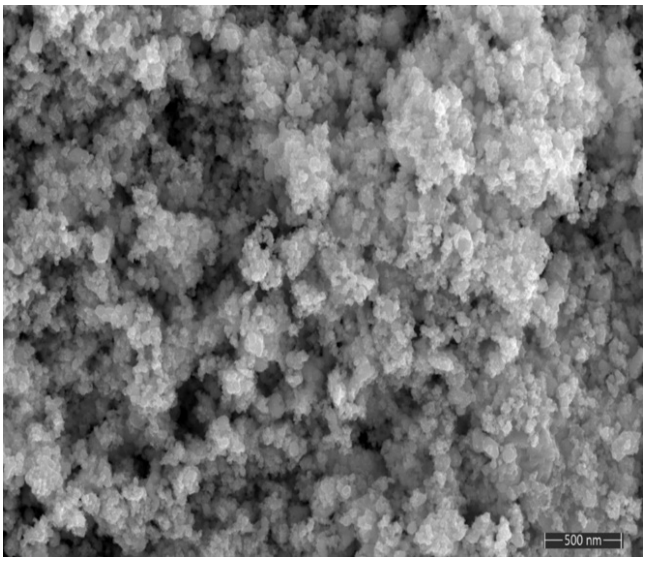


Figure 10. SEM image of silver nanoparticles showing surface morphology.

distribution between 30 and 60 nm and an average size of 35 nm.

3.6.6 Characterization by Energy-dispersive X-ray (EDX)

The energy dispersive spectrum of the produced nanoparticles is displayed in Figure 11, indicating that silver is a component element. Because of surface

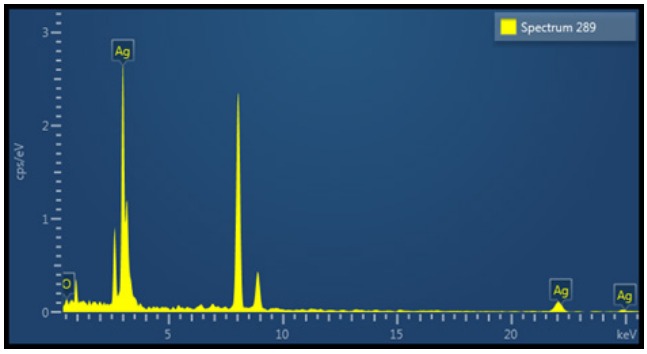


Figure 11. EDX spectrum confirming the elemental composition of synthesized silver nanoparticles.

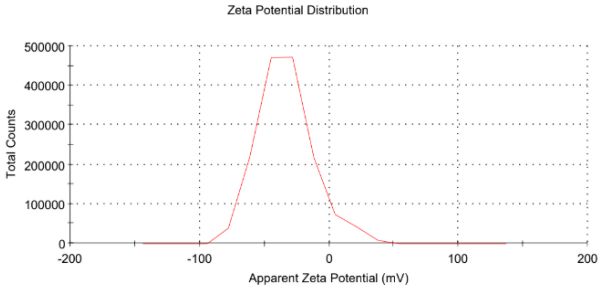


Figure 12. Zeta potential measurement used to assess the surface charge and dispersion stability of synthesized AgNPs.

plasmon resonance, metallic silver nanoparticles often exhibit a significant signal peak around 3 keV. The quantitative data of biosynthesized AgNPs are displayed in Table 4 that illustrates the existence of components like Ag, O, C, K, Cl, Ca, and Na.

3.6.7 Zeta Potential

The zeta potential of the synthesized silver nanoparticles was determined using a Malvern Zetasizer (Model: MAL1111244). The results showed a mean zeta potential value of -33.6 mV. This negative surface charge indicates that the nanoparticles have strong colloidal stability due to enough electrostatic repulsion, which helps to prevent agglomeration in suspension. The study revealed a single, dominating signal with a 100% area distribution, indicating a uniform surface charge throughout the nanoparticle population (Figure 12).

3.7 Antibacterial Activity of Nanoparticle against ESBL- *E. coli*

3.7.1 Antibacterial Activity Using Agar Well Diffusion Assay

The antibacterial efficacy of the biosynthesized AgNPs was evaluated against *E. coli* using the disc diffusion method. As illustrated in Figure 13 a, the AgNPs exhibited pronounced antibacterial activity, indicated by larger inhibition zones compared to the aqueous leaf extract of *T. arjuna*. The maximum inhibition zones were observed at the highest AgNPs concentration, measuring 18 mm against *E. coli* (Figure 13 b). Notably, the AgNPs demonstrated a more potent antibacterial effect against *E. coli* in a dose-dependent manner (Table 5).

Figure 14: Minimum inhibitory concentration silver nanoparticle. Optical Density graph (a) and Percentage Inhibition graph (b)

Figure 15: Percentage viability graph of silver nanoparticle against Vero cell line

Figure 16: Inverted microscope images of Vero cells under control (a) and IC_{50} treatment conditions (b).

3.7.2 Minimum Inhibitory and Bactericidal Concentration

The MIC and MBC was determined using broth dilution method. The MIC and MBC was determined to be 125 and 500 µg/ml respectively (Table 6). The Figure 14 represents OD (a) and Percentage inhibition (b) graph of MIC.

3.8 Cell Cytotoxicity

The cell cytotoxicity of nanoparticle was tested against Vero cell line. The IC_{50} was nanoparticle was reported to be 74.236 µg/ml with percentage viability in the range of 54.83±0.43 to 41.99±0.33 % (Table 7). The Figure 15 and 16 represents the percentage inhibition graph and inverted microscope image of Vero cell: Control (a), IC50 (b).

Table 4. Elements detected by EDX

Element	Line Type	k Factor	Absorption Correction	Wt%	Wt% Sigma	Atomic %
O	K series	2.020	1.00	3.82	1.59	21.11
Ag	K series	10.869	1.00	96.18	1.59	78.89
Total				100.00		100.00

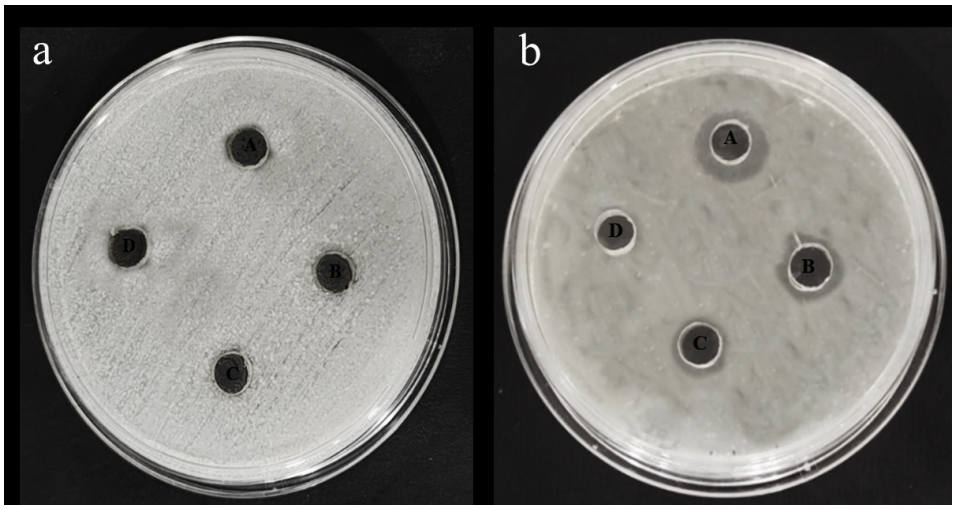


Figure 13. **(a).** Agar well diffusion of plant extract; **(b).** silver nanoparticle.

Table 5. Antibacterial activity using Agar well diffusion assay

Sample	Concentration (µg/ml)			
	1000 (A)	500 (B)	250 (C)	100 (D)
Plant extract	-	-	-	-
Silver nanoparticle	18.50±0.50	14.40±0.53	11.57±0.81	-

Note: Data represents mean values of three replicates ± SD.

Table 6. Percentage bacterial inhibition

S. No	Concentration (µg/ml)	Percentage of Inhibition
1	1000	97.03±0.61
2	500	93.08±0.66
3	250	89.50±0.82
4	125	81.32±0.50
5	62.5	65.87±0.95
6	31.25	54.14±0.57
7	15.62	37.18±0.49
8	7.81	20.05±0.34

Note: Data represents mean values of three replicates ± SD with p value <0.0001.

4. Discussion

Nasal swabs were collected from patients having respiratory infection, then physiological and biochemical tests were carried out to determine bacterial species. In the current study 6 samples were confirmed to be ESBL- producing *E. coli* based on their resistance to third-generation cephalosporins, as observed in antimicrobial susceptibility testing. These isolates exhibited high resistance to cefotaxime and ceftriaxone, confirming β-lactamase activity, while showing susceptibility to colistin and aminoglycosides.

The antibiotic susceptibility testing of six *E. coli* isolates were analyzed based on CLSI breakpoints, by which the strong ESBL- producing isolates (*E. coli*-1, *E. coli*-4, *E. coli*-5, and *E. coli*-6) were categorized as Multidrug-Resistant (MDR) strains, as they exhibited resistance to at least 3 antibiotic classes, including cephalosporins and fluoroquinolones. The mild ESBL-producing isolates (*E. coli*- 2 and *E. coli*- 3) showed intermediate resistance patterns, particularly to cephalosporins, while remaining susceptible to fluoroquinolones and aminoglycosides.

Recent advancements have focused on developing eco-friendly methods for AgNP synthesis, shifting from hazardous chemical processes to biological alternatives. Aligned with green chemistry principles, this study employed an aqueous extract of *T. arjuna* as a reducing agent for AgNP production. Rich in polyphenols, particularly gallic acid, ellagic acid and ellagic acid derivatives, this plant extract offers a promising bio-based approach for AgNP synthesis[20]. Plant-based synthesis offers a sustainable and efficient method for producing silver nanoparticles (AgNPs). This study utilized extracts from *T. arjuna* bark to reduce silver nitrate and form stable AgNPs. The reduction process is primarily driven by flavonoids, which act as potent

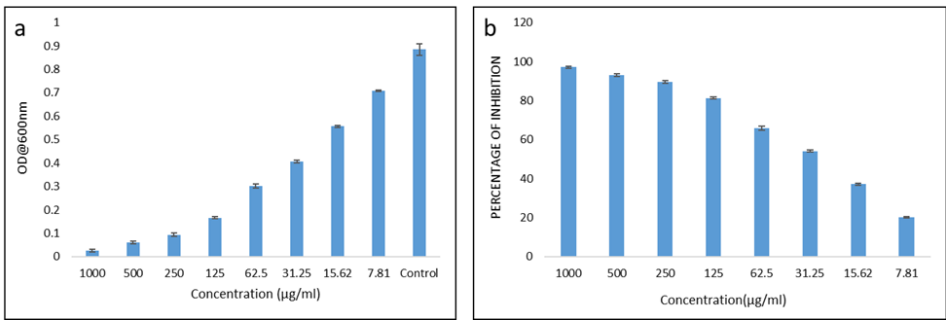


Figure 14. **(a).** Minimum inhibitory concentration silver nanoparticle; **(b).** Optical density graph percentage inhibition graph.

Table 7. Percentage viability of Vero cell line

S. No.	Concentration (µg/ml)	Percentage of Viability	
1	512	23.60±0.26	IC_{50} = 74.236 µg/ml
2	256	35.89±0.63	
3	128	41.99±0.33	
4	64	54.83±0.43	
5	32	61.47±0.50	
6	16	70.41±0.32	
7	8	78.08±0.12	
8	4	86.17±0.58	
9	2	89.23±0.43	
10	1	94.21±0.46	

Note: Data represents mean values of three replicates ± SD with p value <0.0001.

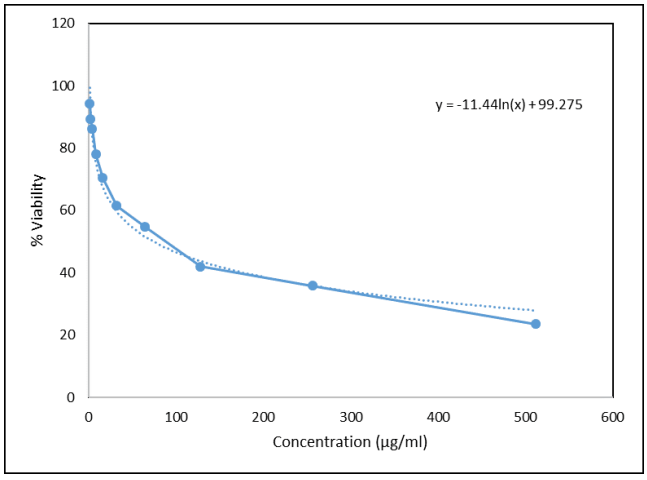


Figure 15. Percentage viability graph of silver nanoparticle against Vero cell line.

reducing agents. These compounds are oxidized as they convert silver ions into nanoparticles. Additionally, the phenolic content of the extract contributes to nanoparticle formation by chelating silver ions[21].

UV-vis spectroscopy is a commonly used technique to track the formation of AgNPs. These nanoparticles exhibit a strong Surface Plasmon Resonance (SPR) absorption band within the 2-100 nm size range. The position of this band shifts towards shorter wavelengths as particle size decreases. Additionally, the surrounding medium and molecules attached to the nanoparticle surface influence the absorption spectrum[22]. According to Mie's theory, spherical nanoparticles produce a single SPR band, whereas non-spherical particles (*e.g.*, rods, triangles, cuboids) generate multiple SPR bands. The aqueous solution containing AgNPs exhibited a reddish-brown color due to the excitation of surface plasmon vibrations within the nanoparticles. The formation of AgNPs from Ag+ ions was monitored using UV-visible spectroscopy.

Proteins and enzymes present in the plant extract also play a crucial role in AgNP synthesis and stabilization. These biomolecules facilitate the reduction of silver ions and form a protective protein corona around the nanoparticles, preventing aggregation. The carboxyl groups within the proteins act as surfactants, enhancing the stability of the AgNPs. Fourier Transform Infrared Spectroscopy (FTIR) analysis confirmed the presence of polyphenols and proteins in the plant extract, supporting their involvement in the formation of AgNPs[23]. The FTIR analysis of *T. arjuna* extract and silver nanoparticles identifies essential functional groups involved in nanoparticle production. The extract has significant peaks at 3818, 3736, and 3218 cm^{-1}, which correspond to free and hydrogen-bonded O-H and N-H groups, indicating the presence of phenolics, flavonoids, and proteins. Carbonyl compounds, alcohols, and amines are confirmed by peaks at 1617, 1381, 1224, and 1051 cm^{-1}, which reflect C=O, C-H, C-O,

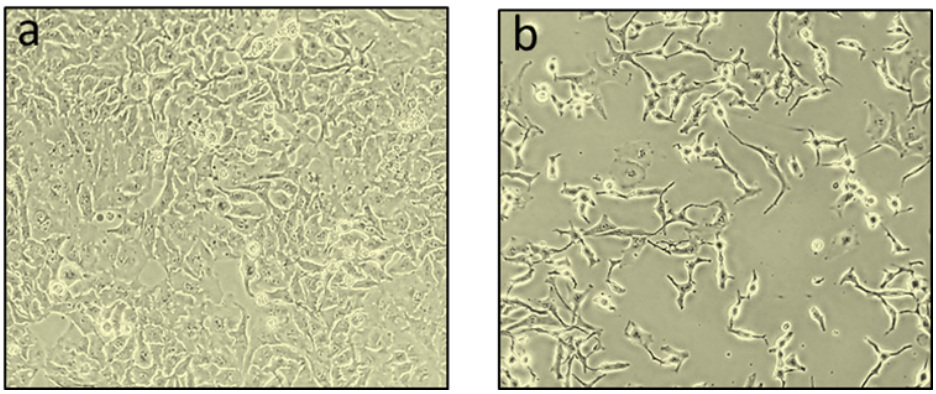


Figure 16. **(a).** Inverted microscope images of Vero cells under control; **(b).** IC_{50} treatment Conditions.

and C-N vibrations respectively. Corresponding peaks shift or develop at 3672, 3283, 2915, 1605, 1501, and 1097 cm^{-1} during nanoparticle formation, indicating the active participation of these groups in both stabilising nanoparticles and reducing Ag^{+} to Ag^{0}. Notably, the proteins and polyphenols roles in reducing and capping the nanoparticles are supported by the shift in the O–H and C=O regions as well as the appearance of peaks linked to amide and aromatic C=C vibrations. *T. chebula*-mediated silver nanoparticles exhibited 2 significant bands in FTIR analysis: One at 3438 cm−1, indicating O-H stretching and H-bonding. Another at 708 cm−1 corresponds to C=C bending[18]. Another study revealed peaks at 3300.34 and 3306.12 cm^{-1}, indicating O-H stretching vibrations from alcohols, phenols, or hydroxyl compounds. Peaks at 2104.19 and 2126.86 cm^{-1} indicate C≡C stretching, while peaks at 1638.15 and 1636.18 cm^{-1} represent C=C and N-H stretching vibrations, respectively[24]. These findings demonstrate that *T. arjuna* phytochemicals function as organic stabilizing and reducing agents when silver nanoparticles are being synthesised.

The crystalline structure and size of synthesized nanoparticles were analyzed using XRD technique, from which average crystalline size was found to be 35nm. Transmission Electron Microscopy (TEM) (Figures 9) and Scanning Electron Microscopy (SEM) (Figure 10) are the most commonly used techniques to provide information regarding morphology, shape, size, composition, and crystallography of the synthesized nanoparticles. The TEM and SEM images have shown that the AgNPs are mostly spherical or quasi-spherical in shape. These results are similar to results in previous literatures by Vishwajeet *et al*[25]. The presence of silver nanocrystals is confirmed by the energy-dispersive X-ray spectra (Figure 11), which displays a prominent absorption peak in the silver region (Lα1) at 3 KeV. Additionally, the presence of the oxygen element was confirmed by the observation of a modest absorption peak in the oxygen area (Kα1) at 0.5 KeV. These results correlate with the findings of Sujitha V *et al*[26].

Silver ions (Ag^{+}) exert antimicrobial effects via affecting ATP generation, harming DNA, and inhibiting respiratory enzymes. Ag^{+} can produce Reactive Oxygen Species (ROS) and interact with thiol groups in proteins, disrupting vital biological activities. Structural damage includes cell wall rupture, DNA condensation, and intracellular content leaking. Even at low concentrations (μM to mM), these effects suppress microbial growth[27]. *Terminalia* AgNPs outperformed crude extracts in terms of bactericidal activity by a factor of at least 20 fold. The increase in antimicrobial-resistant bacterial species supports the need for alternative antibacterial agents[28]. Chemically synthesized AgNPs had a broader size range, no antioxidant activity, and weaker antibacterial and DNA cleavage effects. Green synthesis resulted in more desirable nanoparticles with enhanced biological properties[29]. Silver nanoparticles (AgNPs) have demonstrated potent antibacterial activity against a broad spectrum of bacteria, including multidrug-resistant strains. *T. bellirica* and *T. chebula*- mediated silver nanoparticles demonstrated MIC concentrations of 78-156 μM and 1 mg/ml in investigated *E. coli* strains[30]. Silver nanoparticles capped with *T. catappa* leaf extract (TCE-AgNPs) were synthesized in sizes of 10.60, 4.73, and 3.48 nm (Ag-1, Ag-2, Ag-3). Decreasing particle size enhanced antibacterial activity against MDR *P. aeruginosa*. MIC/MBC values reduced from 7.77/15.54 μg/mL (Ag-1) to 3.88/7.77 μg/mL (Ag-2 and Ag-3) (31). The present study with MIC of 125μg/ml was found to be effective.

Ag-NPs synthesized using *Taxus yunnanensis* Callus extract showed an IC_{50} of 81.39 µg/mL for normal liver cells (HL-7702), while significantly lower IC_{50} values were observed for cancer cell lines A549 (40.3 µg/ml) and MCF-7 (42.2 µg/ml)[32]. Another study revealed that the Silver Nanoparticles synthesized using *Echinochloa stagnina* showed lowest toxicity with IC50 of 89.01 µg/ml against Normal Vero cell line[33]. Compared to previous studies, the cytotoxicity of nanoparticle synthesized using *T. arjuna* was relatively lower, hence it can be considered to be safe.

5. Conclusion

A rapid and environmentally friendly one-step method for synthesizing AgNPs using *T. arjuna* extract has been developed. The polyphenols present in the extract, specifically hydrolysable tannins, act as both reducing and stabilizing agents for AgNP formation. This green approach offers a viable alternative to conventional chemical reduction methods by eliminating the use of toxic chemicals. The synthesized AgNPs demonstrated antimicrobial efficacy against tested MDR bacterial strains. This environmentally benign process holds potential for diverse applications in both medicine and technology.

6. Acknowledgment

The authors gratefully acknowledge Department of Microbiology, Dr. N.G.P Arts and Science College, Bharathiyar University and Simbioen Labs and Scientific Services Private Limited for providing research support.

7. Author Contribution

P. Senthilkumar: Conception and design, writing, collection, research data management. J. Rengaramanujam: Visualisation, oversight, leadership. All authors have read and agreed to the published version of the manuscript.

8. References

1. Sharma S, Chauhan A, Ranjan A, Mathkor DM, Haque S, Ramniwas S, *et al.* Emerging challenges in antimicrobial resistance: Implications for pathogenic microorganisms, novel antibiotics, and their impact on sustainability. Front Microbiol. 2024; 15:1403168. https://doi.org/10.3389/fmicb.2024.1403168
2. Gandhi M, Amreen K. Emerging trends in nanomaterial-based biomedical aspects. Electrochem. 2023; 4(3):365-388. https://doi.org/10.3390/electrochem4030024
3. Chavali MS, Nikolova MP. Metal oxide nanoparticles and their applications in nanotechnology. SN Appl Sci. 2019; 1(6):607.
4. Abuzeid HM, Julien CM, Zhu L, Hashem AM. Green synthesis of nanoparticles and their energy storage, environmental, and biomedical applications. Crystals. 2023; 13(11):1576. https://doi.org/10.3390/cryst13111576
5. Ying S, Guan Z, Ofoegbu PC, Clubb P, Rico C, He F, *et al.* Green synthesis of nanoparticles: Current developments and limitations. Environ Technol Inno. 2022; 26:102336.
6. Dwivedi S, Chopra D. Revisiting *Terminalia arjuna*-An ancient cardiovascular drug. J Tradit Complement Med. 2014; 4(4):224-231. https://doi.org/10.4103/2225-4110.139103
7. Swedan S, Alabdallah EA, Ababneh Q. Resistance to aminoglycoside and quinolone drugs among *Klebsiella pneumoniae* clinical isolates from Northern Jordan. Heliyon. 2024; 10(1): e23368. https://doi.org/10.1016/j.heliyon.2023.e23368
8. Wright MH, Adelskov J, Greene AC. Bacterial DNA extraction using individual enzymes and phenol/chloroform separation. J Microbiol Biol Educ. 2017; 18(2):12-18. https://doi.org/10.1128/jmbe.v18i2.1348
9. Lalzampuia H, Dutta TK, Warjri I, Chandra R. PCR-based detection of extended-spectrum β-lactamases (bla CTX-M-1 and bla TEM) in *Escherichia coli, Salmonella* spp. and *Klebsiella pneumoniae* isolated from pigs in North Eastern India (Mizoram). Indian J Microbiol. 2013; 53:291-296. https://doi.org/10.1007/s12088-013-0378-z
10. Desai D, Chanda S. Pharmacognostic study and physicochemical analysis of leaves of *Terminalia arjuna*. Pharmacog J. 2014; 6(6):15-19. https://doi.org/10.5530/pj.2014.6.4
11. Ahmed S, Ikram S. Silver nanoparticles: One pot green synthesis using *Terminalia arjuna* extract for biological application. J Nanomed Nanotechnol. 2015; 6(4):1-6. https://doi.org/10.4172/2157-7439.1000309
12. Ashraf JM, Ansari MA, Khan HM, Alzohairy MA, Choi I. Green synthesis of silver nanoparticles and characterization of their inhibitory effects on AGEs formation using biophysical techniques. Sci Rep. 2016; 6(1):1-10. https://doi.org/10.1038/srep20414
13. Mulligan SK, Speir JA, Razinkov I, Cheng A, Crum J, Jain T, *et al.* Multiplexed TEM specimen preparation and analysis of plasmonic nanoparticles. Microsc Microanal. 2015; 21(4):1017-1025. https://doi.org/10.1017/s1431927615014324

14. Baudot C, Tan CM, Kong JC. FTIR spectroscopy as a tool for nano-material characterization. Infrared Phys Tech. 2010; 53(6):434-438. https://doi.org/10.1016/j.infrared.2010.09.002
15. Ali MH, Azad MAK, Khan KA, Rahman MO, Chakma U, Kumer A. Analysis of crystallographic structures and properties of silver nanoparticles synthesized using PKL extract and nanoscale characterization techniques. ACS Omega. 2023; 8(31):28133-28142. https://doi.org/10.1021/acsomega.3c01261.s001
16. Kamshad M, Talab MJ, Beigoli S, Sharifirad A, Chamani J. Use of spectroscopic and zeta potential techniques to study the interaction between lysozyme and curcumin in the presence of silver nanoparticles at different sizes. J Biomol Struct Dyn. 2019; 37(8):2030-2040. https://doi.org/10.1080/07391102.2018.1475258
17. Manandhar S, Luitel S, Dahal RK. In vitro antimicrobial activity of some medicinal plants against human pathogenic bacteria. J Trop Med. 2019;2019(1):1895340.
18. Tharani M, Rajeshkumar S, Ghanim KAA, Nicoletti M, Sachivkina N, Govindarajan M. *Terminalia chebula*-assisted silver nanoparticles: Biological potential, synthesis, characterization, and ecotoxicity. Biomedicines. 2023; 11(5):1472. https://doi.org/10.3390/biomedicines11051472
19. Sirisa-ard P, Pholsonklam K, Satchachai A, Tragoolpua Y, Kaewkod T. Antioxidant, antibacterial activities and cytotoxicity of garlic leaf extract from garlic waste. Nat Life Sci Commun. 2023; 22:e2023059. https://doi.org/10.12982/NLSC.2023.059
20. Liaqat N, Jahan N, Anwar T, Qureshi H. Green synthesized silver nanoparticles: Optimization, characterization, antimicrobial activity, and cytotoxicity study by hemolysis assay. Front Chem. 2022; 10:952006. https://doi.org/10.3389/fchem.2022.952006
21. Ahmed Q, Gupta N, Kumar A, Nimesh S. Antibacterial efficacy of silver nanoparticles synthesized employing *Terminalia arjuna* bark extract. Artif Cells Nanomed Biotechnol. 2017; 45(6):1192-1200. https://doi.org/10.1080/21691401.2016.1215328
22. Alzahrani E. Colorimetric detection based on localized surface plasmon resonance optical characteristics for sensing of mercury using green-synthesized silver nanoparticles. J Anal Methods Chem. 2020. https://doi.org/10.1155/2020/6026312
23. Xu L, Wang YY, Huang J, Chen CY, Wang ZX, Xie H. Silver nanoparticles: Synthesis, medical applications and biosafety. Theranostics. 2020; 10(20):8996-9031. https://doi.org/10.7150/thno.45413
24. Singh S, Arya H, Sahu W, Reddy KS, Nimesh S, Alotaibi BS, *et al*. Green synthesized silver nanoparticles of *Terminalia bellirica* leaves extract: Synthesis, characterization, *in-silico* studies, and antimalarial activity. Artif Cells, Nanomed Biotechnol. 2024; 52(1):238-249. https://doi.org/10.1080/21691401.2024.2339429
25. Vishwajeet S, Ankita S, Nitin W. Biosynthesis of silver nanoparticles by plants crude extracts and their characterization using UV, XRD, TEM and EDX. Afr J Biotechnol. 2015; 14(33):2554-2567. https://doi.org/10.5897/ajb2015.14692
26. Sujitha V, Murugan K, Paulpandi M, Panneerselvam C, Suresh U, Roni M, *et al*. Green-synthesized silver nanoparticles as a novel control tool against Dengue virus (DEN-2) and its primary vector *Aedes aegypti*. Parasitol Res. 2015; 114(9):3315-3325. https://doi.org/10.1007/s00436-015-4556-2
27. Kalwar K, Shan D. Antimicrobial effect of silver nanoparticles (AgNPs) and its mechanism- a mini review. Micro Nano Lett. 2018; 13(3):277-280. https://doi.org/10.1049/mnl.2017.0648
28. Majoumouo MS, Sibuyi NRS, Tincho MB, Mbekou M, Boyom FF, Meyer M. Enhanced anti-bacterial activity of biogenic silver nanoparticles synthesized from *Terminalia mantaly* extracts. Int J Nanomedicine. 2019: pp. 9031-9046. https://doi.org/10.2147/ijn.s223447
29. Khattat MM, Keyhanfar M, Razmjou A. A comparative study of stability, antioxidant, DNA cleavage and antibacterial activities of green and chemically synthesized silver nanoparticles. Artif Cells Nanomedicin Biotechnol. 2018; 46(Sup 3):1022-1031. https://doi.org/10.1080/21691401.2018.1527346
30. Ranjani S, Hemalatha S. Nanoformulation target virulence genes to break antibiotic resistance in MDR *E. coli*. Appl Nanosci. 2023; 13(8):5615-5626. https://doi.org/10.1007/s13204-023-02782-w
31. Ansari MA, Kalam A, Sehemi AGA, Alomary MN, AlYahya S, Aziz MK, *et al*. Counteraction of biofilm formation and antimicrobial potential of *Terminalia catappa* functionalized silver nanoparticles against *Candida albicans* and multidrug-resistant Gram-negative and Gram-positive bacteria. Antibiotics. 2021; 10(6):725. https://doi.org/10.3390/antibiotics10060725
32. Xia QH, Ma Y, Wang J. Biosynthesis of silver nanoparticles using *Taxus yunnanensis* callus and their antibacterial activity and cytotoxicity in human cancer cells. Nanomaterials. 2016; 6(9):160. https://doi.org/10.3390/nano6090160
33. Shehabeldine AM, Elbahnasawy MA, Hasaballah AI. Green phytosynthesis of silver nanoparticles using *Echinochloa stagnina* extract with reference to their antibacterial, cytotoxic, and larvicidal activities. BioNanoScience. 2021; 11:526-538. https://doi.org/10.1007/s12668-021-00846-1